CREIM: Coffee Ring Effect Imaging Model for Monitoring Protein Self-Assembly *in Situ*

Michael Shaw,[1,2] *Angelo Bella*[1] *and Maxim G Ryadnov*[1]*

[1]National Physical Laboratory, Hampton Road, Teddington, TW11 0LW, UK

[2]Department of Computer Science, University College London, London, WC1 6BT, UK

Corresponding author:

Dr Maxim G Ryadnov

National Physical Laboratory,

Hampton Road, Teddington, TW11 0LW, UK

Fax: (+44) 20 86140573

Tel: (+44) 20 89436078

max.ryadnov@npl.co.uk

ABSTRACT: protein self-assembly is fundamental to nanotechnology. Self-assembling structures are produced under static *in vitro* conditions typically forming over hours. In contrast, hydrodynamic intra-cellular environments employ far shorter timescales to compartmentalize highly concentrated protein solutions. Herein, we exploit the radial capillary flow within a drying sessile droplet (the coffee ring effect) to emulate dynamic native environments and monitor an archetypal protein assembly *in situ* using high-speed super-resolution imaging. We demonstrate that the assembly can be empirically driven to completion within minutes to seconds without apparent changes in supramolecular morphology. The model offers a reliable tool for the diagnosis and engineering of self-assembling systems under non-equilibrium conditions.

TOC GRAPHIC:

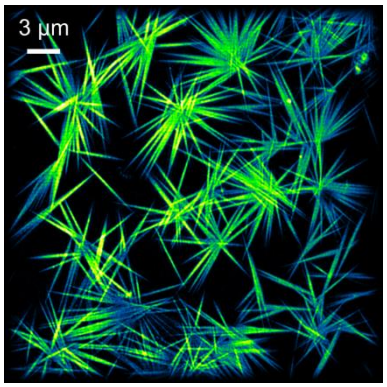

Protein self-assembly is characterised by a spontaneous propagation of polypeptide chains into higher-order supramolecular structures.[1] In biology such polymerization must be driven to completion to avoid monomer redundancy, which may lead to aberrant or toxic oligomers.[2-4] The cell employs molecular crowding to accelerate protein association by excluding solvent volume accessible to co-solute molecules,[5] which can also promote aggregation should misfolding take place.[6] Such an undesired scenario is partially mitigated by the precise encoding of assembly patterns in amino-acid sequences.[7] In addition, intracellular environments are non-equilibrium systems designed to accommodate cell surface tension,[8] with hydrodynamic forces generating flow vortices sustaining monomer mixing.[9] Self-assembly performed under static *in vitro* conditions presents an entirely different situation.[5] It is devoid of hydrodynamic factors and supports systems equilibrated with monomers,[10, 11] which is in contrast to *in cellulo* media that, albeit compartmentalized, are highly concentrated protein solutions.[12,13] Alternative approaches aiming to emulate assembly kinetics include the use of concentrated cell extracts or high concentrations of co-solutes to mimic molecular crowding.[5, 14-16] However, none of these strategies allows for the direct observation of protein self-assembly under hydrodynamic conditions, free of the complexity of live cell measurements. Herein we report a method for monitoring protein self-assembly in the regime of dynamic molecular crowding at protein concentrations typical of live cells.[17] Our approach (CREIM) makes use of the coffee ring effect (CRE), which introduces a concentration gradient in a drying sessile droplet,[18] and high speed time-lapse super-resolution fluorescence microscopy for quantitative imaging of protein self-assembly at the droplet edges.

Although ubiquitous for various systems with constituents as diverse as colloidal composites and bacterial cells,[19-21] CRE has yet to be shown for a hierarchical, living assembly process. For a drying sessile droplet in which the droplet edge is pinned to the substrate, evaporative solvent loss can result in radial capillary flow. This flow drives suspended particles out to the

droplet edge forming a characteristic (coffee) ring deposit. In the idealised case the effect depends only on the droplet radius and the contact angle.[18] In practice, however, it can be supressed by gradients in surface tension created by Marangoni flows.[22, 23] Synthetic and biological surfactants effectively reverse CRE by inducing vortices in the droplet,[21, 24] while uniform drying deposits are created using ellipsoidal particles and by modifying particle-particle and particle-substrate interactions.[25, 26] Similarly, self-assembling structures rely on an interplay between the hydrophobic effect and oppositely charged interactions of assembling monomers.

This interplay underpins the transformation from a disordered molecule to an ordered microscopic material of a well-defined shape. Two main phases for protein assembly can be distinguished – passive (monomeric) and polymerized, or in the context of the classical nucleation theory – sub-nuclei and super-nuclei. A critical question remains as to whether persistent crowding, induced by a concentration gradient, shifts equilibrium to assembly or favours misfolding and aggregation.

Results and Discussion

With this in mind, we monitored the assembly of an archetypal α-helical protein filament in a sessile droplet (Fig 1A). The filament, previously introduced as a fibrillogenesis imaging model (FiM),[27] assembles from a de novo coiled-coil sequence into anisotropic fibrillar structures of ~ 2.5 μm in length (Fig 1B, and S1A in Supporting Information).

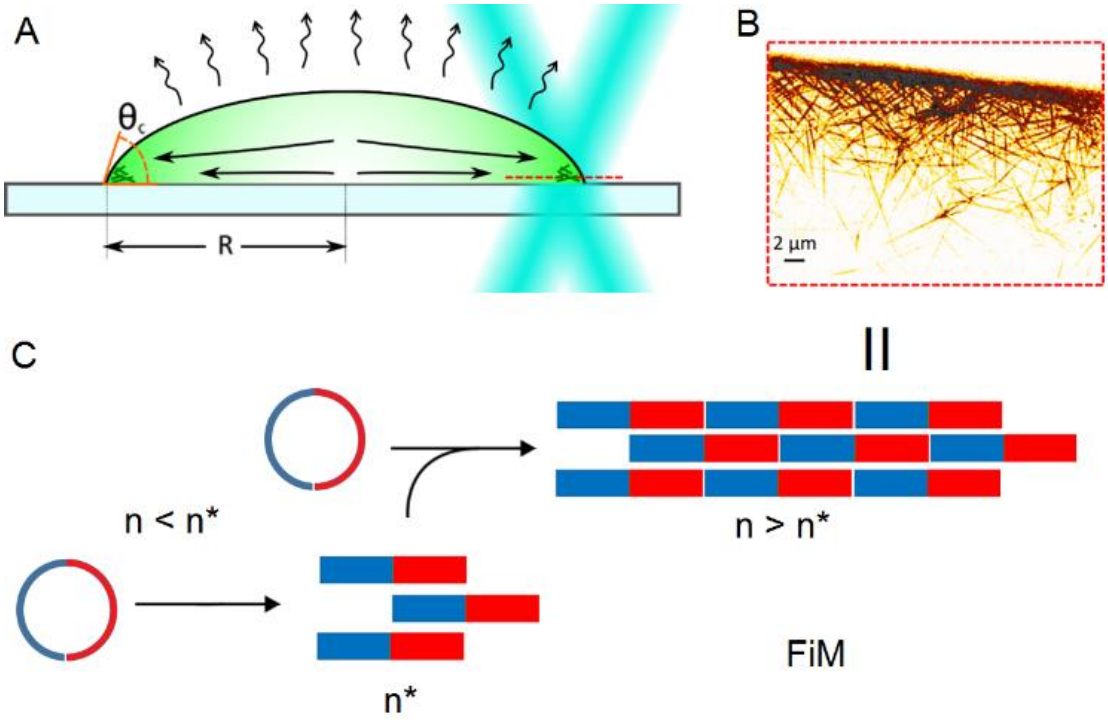

Fig. 1. Coffee ring effect imaging model (CREIM). (A) A schematic of CREIM monitoring of filamentous protein assembly. Curly and horizontal arrows denote evaporative flux and a radial capillary flow towards the edge of a droplet. In the idealised case, this outward flow depends only on the droplet radius (R) and the droplet contact angle (Θ_c) (see Supporting Information). Interference of two fluorescence excitation beams (cyan) creates a sinusoidal illumination pattern at the droplet edge for structured illumination imaging. (B) A representative micrograph of filaments forming at the edge of the droplet. (C) A schematic of the assembly. Circles and rectangles denote assembly-passive (unordered) and assembly-committed (folded) monomers, respectively, each comprising complementary cationic (blue) and anionic (red) halves. The halves of different monomers co-fold, bundling up into α-helical coiled coils. n* is a nuclei phase (assembly active), while n < n* and n > n* are sub-nuclei and super-nuclei phases, respectively.

The assembly completes within 4 hours with the same growth rates at both ends of propagating filaments. Unlike β-pleated or amyloid-like fibrils, which are characterized by structural polymorphism and large heterogeneities in growth kinetics,[28] FiM produces statistically significant densities of uniformly sized assemblies.[27] To visualize the assembly process we used high-speed structured illumination microscopy (SIM). This is a widefield fluorescence

imaging technique in which spatial resolution is increased beyond the classical diffraction limit by illuminating the sample with patterned light (Fig 1A).[29] In order to maximise imaging speed to capture the dynamics of self-assembly we generated illumination patterns using a fast switching liquid crystal on silicon spatial light modulator, while reducing the number of raw image frames required for each super-resolution image by removing the out of focus light in each plane during image reconstruction.[30] This enabled fast optically sectioned imaging with a lateral spatial resolution (Rayleigh criterion) of ~ 130 nm and an optical section thickness of 500 nm - 600 nm.

In contrast to other super-resolution imaging methods SIM does not impose additional constraints on fluorophore properties, which proves beneficial for imaging fluorescently labelled monomers that can co-assemble with unlabelled monomers at low ratios.[27] Combined with the CRE, the designed method offers an integrated model allowing for the monitoring of protein self-assembly *in situ*, which we refer to as a CRE imaging model (CREIM).

We used CREIM to monitor self-assembly in a 5 µL droplet of FiM mixed with FiM-Alexa Fluor 488 in a molar ratio $1:10^{-3}$. Near the droplet edge full-length filaments (2.5 µm) formed within the droplet drying time of 30 min. Individual filaments were found to form within 4-6 minutes (Movie S1), which is in stark contrast to the period of 4 hours that was necessary under static conditions (Fig 2, Fig S2A, B and Movie S2). Elongation rates for these filaments were at least two orders of magnitude higher than those for filaments grown in solution (Fig S2C). The growth mode of FiM in the droplet was yet identical to those observed in solution, at the same ratios and peptide chain concentrations. Individual filaments propagated uniformly from both termini forming dense carpets. The carpets were evident near the droplet edges regardless

of the initial volume used (Fig 3A), confirming that CRE does not appear to affect the morphology of the assembled filaments (Figs 2, 3 and S1).

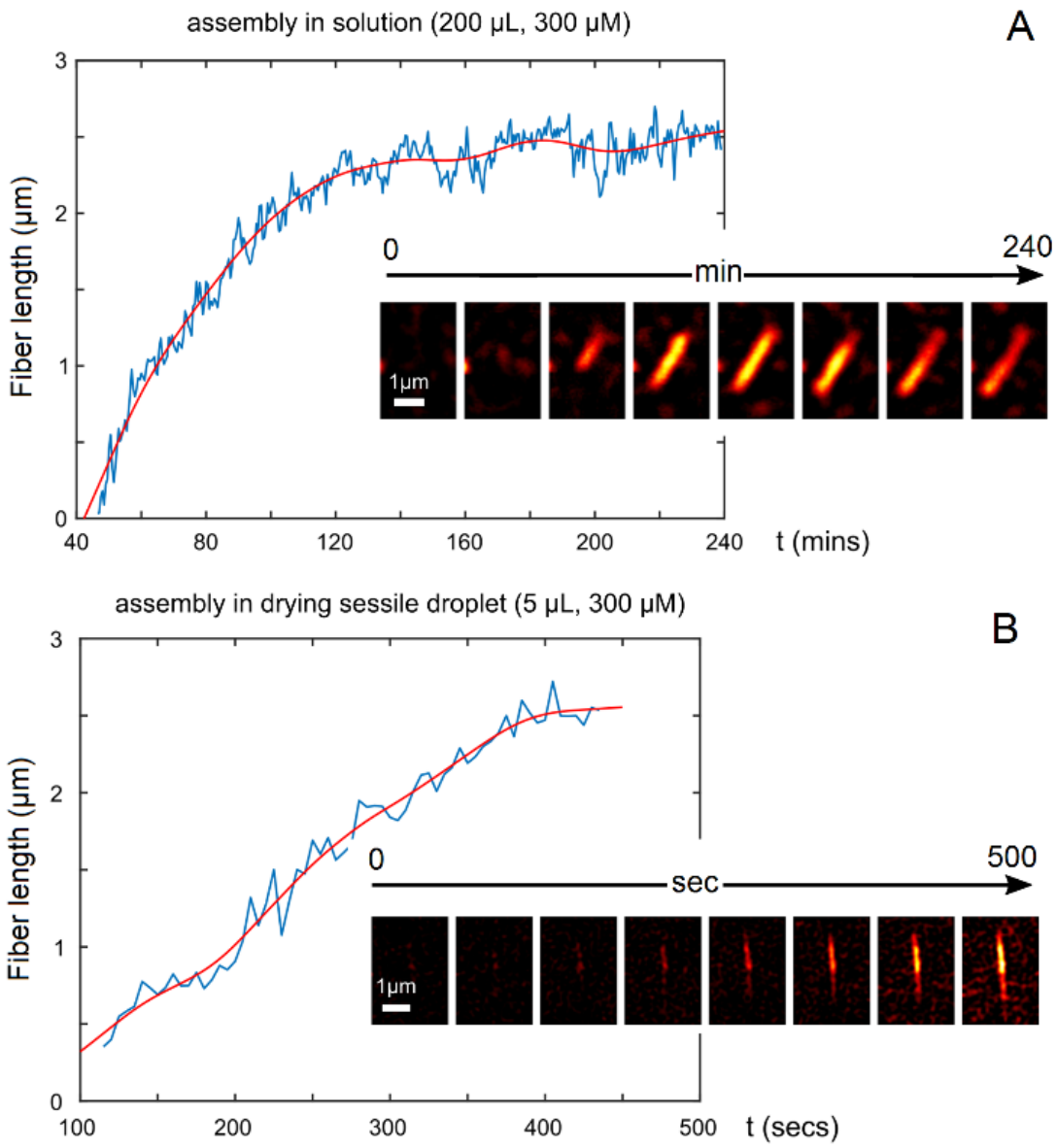

Fig. 2. Comparative assembly kinetics. The growth of individual FiM filaments in a static (equilibrated) solution (A) and near the contact line of a drying sessile droplet (B). Red curves show smoothing splines fitted to the raw length values (blue). Image montages show selected frames from the total time-lapse image sequences analysed to compute fiber length versus time.

As expected, the deposition area (ring thickness) was greater for droplets with a larger initial volume (Fig 3B). For smaller droplets the assembly was complete within as little as 30 seconds from initial droplet formation (Fig 3A). This finding is notable for three reasons.

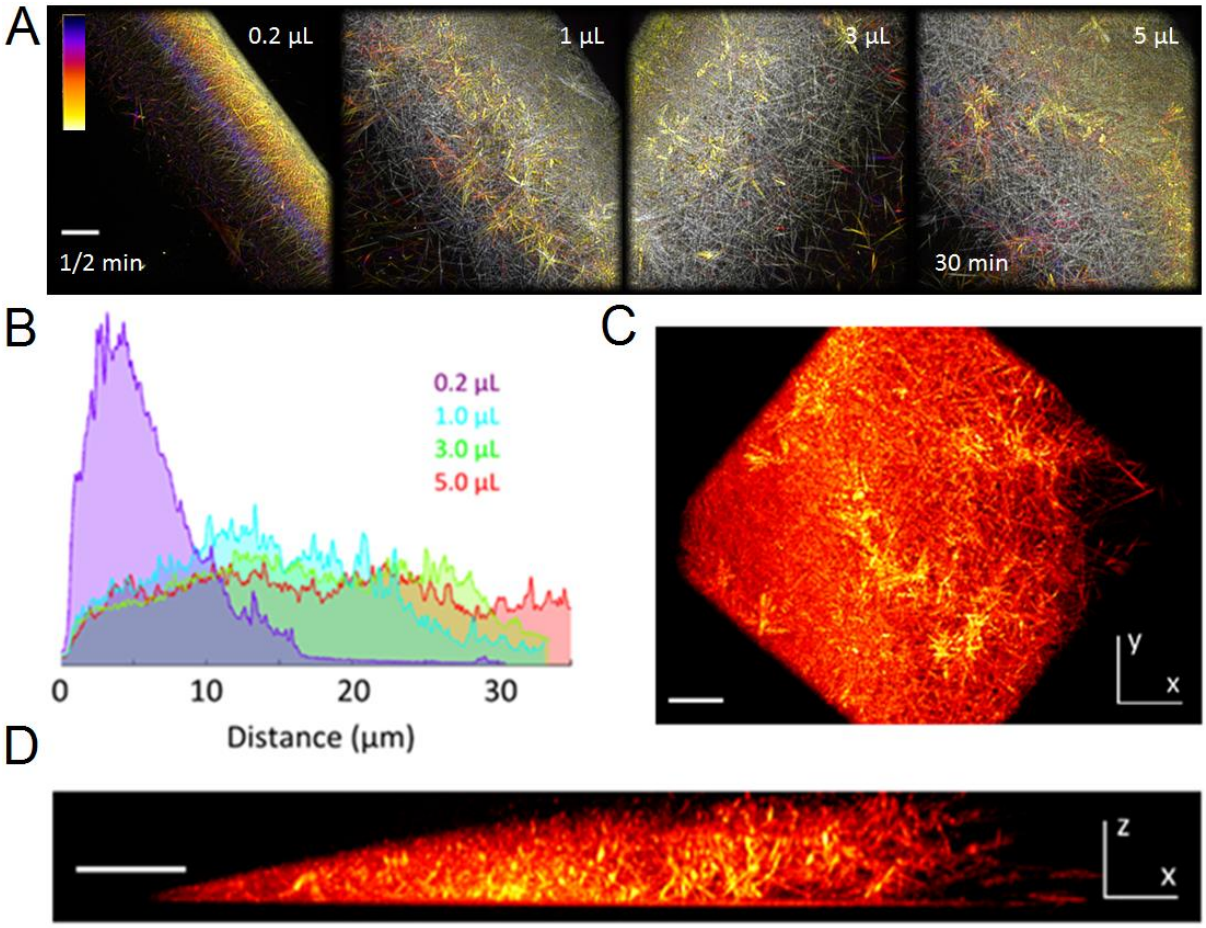

Fig. 3. Complete assembly morphology. (A) Color-coded depth projections showing dense carpets of filaments (100 µM) near the droplet contact line for different initial droplet volumes. The images were taken for dried samples reconstituted to the same initial volume, shown in each image. Times given are those required for the corresponding droplet to fully dry. Color depth scale is 10 µm. (B) Line profiles drawn through normalised maximum intensity projections corresponding to the images in (A) showing wider deposition rings for larger droplet volumes. (C) XY and (D) XZ maximum intensity projections of filaments formed near the droplet edge (5 µL). All scale bars are 5 µm.

Firstly, FiM assembles into a well-defined microscopic phase of positively charged hydrated ellipsoids that can favor propulsion toward the high surface tension side of the droplet.[25] By

interfacing with one another and with air-water and solid-water interfaces self-assembling peptides generate strong and localized Marangoni effects.[31] These may not inhibit CRE as evaporation completes with the phase, but should manifest in a random (unaligned) distribution of the filaments at the drop edges. This was indeed evident during imaging (Fig 3), while some filaments appeared as converging at one end, rather than branching, consistent with previous observations for the assembly in solution (Fig 3A).[27] The filament growth was strongly anisotropic, which is prerequisite for fibrillation, during which lateral growth is arrested at an early stage due to much weaker interactions.[32]

Secondly, during assembly FiM maintains varied hydrophobicity (each monomer is amphipathic), which further supports crowding vortices at the level of an individual growing filament.[33] Under such persistent micro-mixing, the filaments must assemble, as they did, at much faster rates when compared to static conditions (Figs 2 & 3). Such accelerated assembly had no impact on folding, with the morphology of straight filaments preserved. Consistent with homogeneous nucleation models,[34] this retention confirms FiM as an energy-independent hierarchical transition. Typical of other autonomous structures (e.g. intermediate filaments, viruses), FiM filaments complete upon saturation, whereas super-saturation does not affect their growth kinetics or morphology. In the ring region of a drying droplet the mass of solute material increases exponentially as defined by the initial volume of the droplet and its drying rate (Supplementary Information). For systems that do not undergo hierarchical transitions, e.g. fluorescent nanoparticles, CRE merely concentrates solute material at the droplet periphery (Fig S3). The particles pack closely at the contact line resulting in uniform depositions upon drying. For FiM, the amount of material also remains constant but the material itself transforms from one phase (peptide) to another (filament). Monomers are depleted due to incorporation into filaments whose mass increases. This process indicates that CRE endows *in vitro* measurements with hydrodynamic conditions reminiscent of native environments.

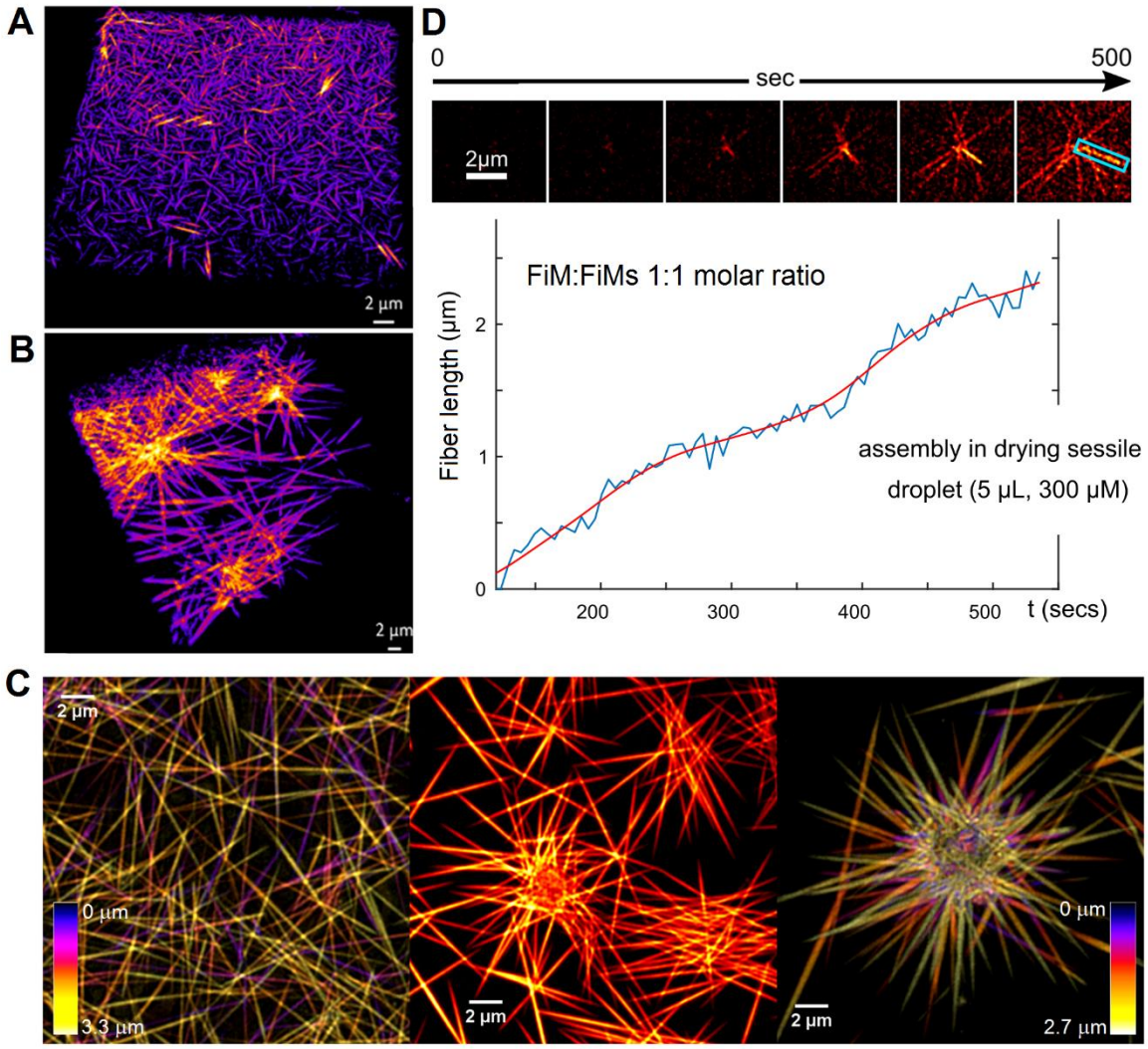

Fig. 4. Comparative assembly morphology for a two-component system. False color perspective views of filaments assembled near the contact line of dried droplets (5 µL) for (A) FiM:FiM-Alexa Fluor 488 (1:10^{-3} molar ratio) and (B) FiM:FiM-Alexa Fluor 488 (1:10^{-3} molar ratio) mixed with FiMs at a 2:1 molar ratio. (C) SIM images for FiM:FiM-Alexa Fluor 488 (1:10^{-3} molar ratio) mixed with FiMs at different molar ratios (from left to right): 30:1, 2:1 and 1:1. The images are shown as color coded depth projections (left and right) and a maximum intensity projection (middle). (D) The growth of an individual filament (blue rectangle) in a star structure near the contact line of a drying sessile droplet. Image montage shows selected frames from the total time-lapse image sequences analyzed to compute fiber elongation versus time. Red curve shows a smoothing spline fitted to the raw length values (blue).

Thirdly, the alternative of non-specific aggregation is excluded by the fact that the assembly is specified at both primary (amino acids sequences) and secondary (sticky-ended coil coil) structure levels. The results thus strongly suggest that monomers in homogeneous systems assemble instantaneously and strictly according to the pathways pre-determined in their sequences. Conversely, proteins that do not self-assemble are not expected to assemble under the CRE conditions. Indeed, the perfectly autonomous β-can fold of green fluorescent protein (GFP)[35] did not propagate under the conditions (Fig S4A). This suggests that the assembly rates observed during CREIM better reflect those in native self-assembly environments and that complementary assembly modes can be introduced and monitored in the same system.[36] To probe this, FiM:FiM-Alexa Fluor 488 ($1:10^{-3}$ molar ratio) was imaged as a 2:1 molar mixture with a specialist peptide, termed FiM star (FiMs). FiMs is the N-terminal cationic fragment of the FiM sequence duplicated in a tail-to-tail fashion via a flexible linker.[10] It is complementary to the C-terminal anionic fragment of the FiM sequence, which requires two FiM copies for the specialist to fully fold (Fig S1B). Similar to GFP the peptide cannot assemble or indeed co-assemble with FiM at infinitely higher ratios (FiM:FiMs $1:10^{3}$). No high order structures, but non-specific aggregates, could be observed for these (Fig S4B). At ratios equimolar or lower, FiMs can appreciably impact on the standard filament morphology (Fig 4A), by introducing a compatible co-assembly mode (Fig 4B, C).

More specifically, a coiled coil resulting from the co-assembly of FiM and FiMs has two identical growing ends, both cationic, which is in contrast to FiM coiled coils whose ends are oppositely charged (Fig S1B). FiMs acts as a hub that pins the standard FiM assembly to one end, driving filament growth from the N-termini. Without fully converting the assembly into a unipolar mode, the specialist can incorporate at any point of FiM assembly, owing to the flexible linkers joining its two assembly-active halves (Fig S1B). Consequently, the peptide increases the strength of lateral interactions contributing to the thickening of growing filaments

that at lower FiMs ratios should be and were noticeably longer (Fig 4C).[10] At ratios close to equimolar FiMs is prone to introduce nucleation sites allowing for the radial assembly of multiple fibers resulting in the formation of star-shaped structures (Fig 4C). The growth rate of individual fibers in these structures was found to be comparable to that for the standard FiM assembly (Figs 4D and S2C, D). With the clearly visible nucleation sites, the star structures had substantially longer and fewer filaments. The feature is attributed to the formation of a secondary nucleation phase[36] at the expense of increased thickening catalyzed by FiMs. This however should be distinguished from heterogeneous nucleation events typical of amyloid, which occur randomly on amyloid surfaces giving rise to polymorphic assemblies.[28,34] By contrast, the two-component FiM:FiMs assembly remains homogeneous as it has two distinct morphologies – straight filaments, albeit larger, and star-like hubs.

Collectively our results prompt a number of key conclusions. First of all, CREIM unequivocally revealed that protein assembly occurs at substantially faster assembly rates when compared to those of the same system in solution at the same chain concentrations. This renders the method perfectly suited to monitor homogeneous protein self-assembly *in situ*. In practical terms, the method offers an optimal measurement platform to diagnose self-assembling systems under non-equilibrium conditions without the complexity of live intracellular measurements. Similarly, the method is applicable to studying energy-independent self-replicating systems that generate monomers in numbers geometrically proportional to the number of resulting assemblies (e.g. viruses).[37] Interestingly, because such systems have a limited capacity to encode a specific means for migration inside host cells, physical intracellular processes are more important for monitoring their intracellular traffic and release, which CREIM can readily provide.

CREIM is suitable for studying all types of self-assembling shapes, from spherical to filamentous.[38] Exemplified by filamentous forms, the self-assembly kinetics of each assembly

can be described using a straight chain of n monomers. An ordered phase comprising n^* monomers could then constitute a nuclei, with an $n < n^*$ system being sub-nuclei and $n > n^*$ super-nuclei (Fig 1C).[34] FiM assembly agrees well with this convention as in both cases inter-filament associations do not take place. The same discrete formations are characteristic of other homogeneous assemblies, all of which are controlled by monomer attachments and detachments.[32] Therefore, assembly-committed monomers provide the nuclei, which subsequently permits nucleation as a process independent of a super-saturation ratio at which the assembly is effectively complete.[36] Sub-nuclei can be viewed as assembly-passive monomers (e.g. random coil) and nuclei as propagating folding elements (e.g. coiled coils, β-hairpins).[39] This transition from passive to nascent forms is bound to a conformational change of the monomer, from unordered to folded structures, any deviation from which would lead to a heterogeneous assembly. In this vein, CREIM provides a diagnostic tool for the encoding reproducibility of self-assembling amino-acid sequences or indeed topologies, including linear and orthogonal.[38] As demonstrated here, by replicating in small volumes the same sequence-assembly pathways that are observed in bulk, our approach excludes stochastic scenarios.[40] It is free of fluctuations in assembly kinetics for folding-defined systems and hence holds promise for assessing multi-component and compartmentalized assemblies in the same volume. Without being necessarily heterogeneous, such systems incorporate several simultaneous, stepwise or promiscuous modes of assembly.[41] It is of increasing interest to elucidate each mode individually, whether to inhibit or promote it, and to exploit potential synergies between different modes, for which multi-modal imaging regimes based on CREIM may be developed.

Supporting information

Materials and Methods together with additional Tables and Figures as described in the text.

AUTHOR INFORMATION

Corresponding author

max.ryadnov@npl.co.uk

Notes

The authors declare no competing financial interests.

ACKNOWLEDGEMENTS

This work was supported in part by a Capital for Great Technologies grant (EP/K005030/1) from the UK's Engineering and Physical Sciences Research Council and the UK's Department of Energy, Business and Industrial Strategy.

REFERENCES

(1) Marsh, J. A.; Hernández, H.; Hall, Z.; Ahnert, S. E.; Perica, T.; Robinson, C. V.; Teichmann, S. A. Protein Complexes are under Evolutionary Selection to Assemble via Ordered Pathways. *Cell*, **2013**, *153*, 461-470

(2) Brangwynne, C. P.; Tompa, P.; Pappu, R. V. Polymer Physics of Intracellular Phase Transitions. *Nat Phys.*, **2015**, *11*, 899–904.

(3) Michaels, T. C.; Liu, L. X.; Meisl, G.; Knowles, T. P. Physical Principles of Filamentous Protein Self-Assembly Kinetics. *J Phys Condens Matter.*, **2017**, *29*, 153002.

(4) Campioni, S.; Mannini, B.; Zampagni, M.; Pensalfini, A.; Parrini, C.; Evangelisti, E.; Relini, A.; Stefani, M.; Dobson, C. M.; Cecchi, C.; Chiti, F. A Causative Link between the Structure of Aberrant Oligomers and Their Toxicity. *Nat Chem Biol*, **2010**, *6*, 140-147.

(5) Ellis, R. J. Macromolecular Crowding: Obvious but Underappreciated. *Trends Biochem Sci*, **2001**, *26*, 597-604.

(6) van den Berg, B.; Ellis, R. J.; Dobson, C. M. Effects of Macromolecular Crowding on Protein Folding and Aggregation. *EMBO J.*, **1999**, *18*, 6927-6933.

(7) Englander, S. W.; Mayne, L. The Case of Defined Protein Folding Pathways. *Proc Natl Acad Sci USA*, **2017**, *114*, 8253-8258.

(8) Schnell, S.; Turner, T. E. Reaction Kinetics in Intracellular Environments with Macromolecular Crowding: Simulations and Rate Laws. *Prog Biophys Mol Biol*., **2004**, *85*, 235-260.

(9) Keren, K.; Yam, P. T.; Kinkhabwala, A.; Mogilner, A.; Theriot, J. A. Intracellular Fluid Flow in Rapidly Moving Cells. *Nat Cell Biol*., **2009**, *11*, 1219-1224.

(10) Ryadnov, M. G.; Woolfson, D. N. Engineering the Morphology of a Self-Assembling Protein Fibre. *Nat Mater*., **2003**, *2*, 329-332.

(11) Mann, S. Self-Assembly and Transformation of Hybrid Nano-Objects and Nanostructures under Equilibrium and Non-Equilibrium Conditions. *Nat Mater*, **2009**, *8*, 781-792.

(12) Ciryam, P.; Kundra, R.; Morimoto, R. I.; Dobson, C. M.; Vendruscolo, M. Supersaturation is a Major Driving Force for Protein Aggregation in Neurodegenerative Diseases. *Trends Pharmacol Sci*, **2015**, *36*, 72-77.

(13) Homouz, D.; Perham, M.; Samiotakis, A.; Cheung, M. S.; Wittung-Stafshede, P. Crowded, Cell-Like Environment Induces Shape Changes in Aspherical Protein. *Proc Natl Acad Sci USA*, **2008**, *105*, 11754-11759.

(14) Smith, S.; Cianci, C.; Grima, R. Macromolecular Crowding Directs the Motion of Small Molecules Inside Cells. *J R Soc Interface*. **2017**, *14*, pii: 20170047.

(15) Gorensek-Benitez, A. H.; Smith, A. E.; Stadmiller, S. S.; Perez Goncalves, G. M.; Pielak, G. J. Cosolutes, Crowding, and Protein Folding Kinetics. *J Phys Chem B*, **2017**, 121, 6527-6537.

(16) White, D. A.; Buell, A. K.; Knowles, T. P.; Welland, W. E.; Dobson, C. M. Protein Aggregation in Crowded Environments. *J Am Chem Soc.*, **2010**, *132*, 5170-5175.

(17) Ghaemmaghami, S.; Huh, W. K.; Bower, K.; Howson, R. W.; Belle, A.; Dephoure, N.; O'Shea, E. K.; Weissman, J. S. Global Analysis of Protein Expression in Yeast. *Nature* **2003**, *425*, 737-741.

(18) Deegan, R. D.; Bakajin, O.; Dupont, T. F.; Huber, G.; Nagel, S. R.; Witten, T. A. Capillary Flow as the Cause of Ring Stains from Dried Liquid Drops. *Nature* **1997**, *389*, 827-829.

(19) Bigioni, T. P.; Lin, X. M.; Nquyen, T. T.; Corwin, E. I.; Witten, T. A.; Jaeger, H. M. Kinetically Driven Self-Assembly of Highly Ordered Nanoparticle Monolayers. *Nat Mater.*, **2006**, *5*, 265-270.

(20) Deegan, R. D. Pattern Formation in Drying Drops. *Phys Rev E*, **2000**, *61*, 475-485.

(21) Sempels, W.; De Dier, R.; Mizuno, H.; Hofkens, J.; Vermant, J. Auto-Production of Biosurfactants Reverses the Coffee Ring Effect in a Bacterial System. *Nat Commun.*, **2013**, *4*, 1757.

(22) Scriven, L. E.; Sternling, C. V. The Marangoni Effects. *Nature*, 1960, *187*, 186-188.

(23) Deegan, R. D.; Bakajin, O.; Dupont, T. F. Huber, G.; Nagel, S. R.; Witten, T. A. Contact Line Deposits in an Evaporating Drop. *Phys Rev. E*, **2000**, *62*, 756-765.

(24) Still, T.; Yunker, P. J.; Yodh, A. G. Surfactant-Induced Marangoni Eddies Alter the Coffee-Rings of Evaporating Colloidal Drops. *Langmuir*, **2012**, *28*, 4984-4988.

(25) Yunker, P. J.; Still, T.; Lohr, M. A.; Yodh, A. G. Suppression of the Coffee-Ring Effect by Shape-Dependent Capillary Interactions. *Nature*, **2011**, *476*, 308-311.

(26) Anyfantakis, M.; Geng, Z.; Morel, M.; Rudiuk, S.; Baigl, D. Modulation of the Coffee-Ring Effect in Particle/Surfactant Mixtures: the Importance of Particle-Interface Interactions. *Langmuir*, **2015**, *31*, 4113-4120.

(27) Bella, A.; Shaw, M.; Ray, S.; Ryadnov, M. G. Filming Protein Fibrillogenesis in Real Time. *Sci. Rep.* **2014**, *4*, 7529.

(28) Pinosti, D.; Buell, A. K.; Galvagnion, C.; Dobson, C. M.; Kaminski-Schierle, G. S.; Kaminski, C. F. Direct Observation of Heterogeneous Amyloid Fibril Growth Kinetics via Two-Color Super-Resolution Microscopy. *Nano Lett*. **2014**, *14*, 339-345.

(29) Shaw, M.; Zajiczek, L.; O'Holleran, K. High Speed Structured Illumination Microscopy in Optically Thick Samples. *Methods* **2015**, *88*, 11-19.

(30) O'Holleran, K.; Shaw, M. Optimized Approaches for Optical Sectioning and Resolution Enhancement in 2D Structured Illumination Microscopy. *Biomed. Opt. Express*, **2014**, *5*, 2580-2590.

(31) Ikezoe, Y.; Washino, G.; Uemura, T.; Kitagawa, S.; Matsui, H. Autonomous Motors of a Metal-Organic Framework Powered by Reorganization of Self-Assembled Peptides at Interfaces. *Nat Mater.*, **2012**, *11*, 1081-1085.

(32) Kashchiev, D.; Auer, S. Nucleation of Amyloid Fibrils. *J Chem Phys*., **2010**, *132*, 215101.

(33) Anyfantakis, M.; Baigl, D.; Binks, B. P. Evaporation of Drops Containing Silica Nanoparticles of Varying Hydrophobicities: Exploiting Particle-Particle Interactions for Additive-Free Tunable Deposit Morphology. *Langmuir*, **2017**, *33*, 5025-5036.

(34) Kashchiev, D. Protein Polymerization into Fibrils from the Viewpoint of Nucleation Theory. *Biophys J*, **2015**, *109*, 2126-2136.

(35) Zacharias, D. A.; Tsien, R. Y. Molecular Biology and Mutation of Green Fluorescent Protein. *Methods Biochem Anal.*, **2006**, *47*, 83-120.

(36) Ryadnov, M. G.; Woolfson, D. N. Introducing Branches into a Self-Assembling Peptide Fiber. *Angew Chem Int Ed*., **2003**, *42*, 3021-3023.

(37) Bruinsma, R. F.; Gelbart, W. M.; Reguera, D.; Rudnick, J.; Zandi, R. Viral Self-Assembly as a Thermodynamic Process. *Phys Rev Lett*., **2003**, *90*, 248101.

(38) De Santis, E.; Ryadnov, M. G. Peptide Self-Assembly for Nanomaterials: the Old New Kid on the Block. *Chem Soc Rev*., **2015**, *44*, 8288-8300.

(39) Kashchiev, D. Modeling the Effect of Monomer Conformational Change on the Early Stage of Protein Self-Assembly into Fibrils. *J Phys Chem B*, **2016**, *121*, 35-46.

(40) Michaels, T. C.; Dear, A. J.; Kirkegaard, J. B.; Saar, K. L.; Weitz, D. A.; Knowles, T. P. Fluctuations in the Kinetics of Linear Protein Self-Assembly. *Phys Rev Lett*., **2016**, *116*, 258103.

(41) Faruqui, N.; Bella, A.; Ravi, J.; Ray, S.; Lamarre, B.; Ryadnov, M. G. Differentially Instructive Extracellular Protein Micro-Nets. *J Am Chem Soc*, **2014**, *136*, 7889-7898.